

# RSC Advances



This is an *Accepted Manuscript*, which has been through the Royal Society of Chemistry peer review process and has been accepted for publication.

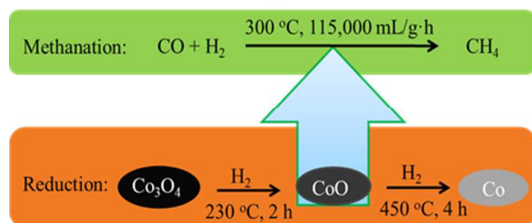
*Accepted Manuscripts* are published online shortly after acceptance, before technical editing, formatting and proof reading. Using this free service, authors can make their results available to the community, in citable form, before we publish the edited article. This *Accepted Manuscript* will be replaced by the edited, formatted and paginated article as soon as this is available.

You can find more information about *Accepted Manuscripts* in the [Information for Authors](#).

Please note that technical editing may introduce minor changes to the text and/or graphics, which may alter content. The journal's standard [Terms & Conditions](#) and the [Ethical guidelines](#) still apply. In no event shall the Royal Society of Chemistry be held responsible for any errors or omissions in this *Accepted Manuscript* or any consequences arising from the use of any information it contains.

### Abstract Graphic

Co<sub>3</sub>O<sub>4</sub> nanoparticles showed high catalytic activity for low temperature CO methanation. CoO is the active phase of the catalyst. Pre-reduction treatment can improve catalytic stability.



## ARTICLE

## Active phase of highly active $\text{Co}_3\text{O}_4$ catalyst for synthetic natural gas production

Cite this: DOI: 10.1039/x0xx00000x

Baowei Wang<sup>\*a</sup>, Sihan Liu<sup>a</sup>, Zongyuan Hu<sup>a</sup>, Zhenhua Li<sup>a</sup>, Xinbin Ma<sup>\*a</sup>Received 00th January 2012,  
Accepted 00th January 2012

DOI: 10.1039/x0xx00000x

www.rsc.org/

$\text{Co}_3\text{O}_4$  catalyst was studied for the methanation in synthetic natural gas (SNG) production. Nanosized  $\text{Co}_3\text{O}_4$  particles were prepared using a facile precipitation method. The different chemical valence states of Co species were obtained by adopting various reduction processes before methanation. The physicochemical properties of catalysts were characterized by  $\text{N}_2$ -physorption, TPR, TEM, XRD, XPS and TG technologies. The catalytic activities for CO methanation were investigated over catalysts with different reduction treatments. Catalyst experienced a mild reduction process with the appearance of CoO species immediately exhibited 100% conversion of CO with a high space velocity of 11500 mL/g·h at 300 °C, 3 MPa. The catalyst without reduction of  $\text{Co}_3\text{O}_4$  achieved the same high activity after 3 h exposure in syngas. When Co oxides were fully reduced to metallic Co, it showed no activity for methanation. Combining the results of characterization with evaluation, it can be concluded that CoO is the active phase for CO methanation. The reduction treatment can improve the stability of catalyst.

### 1. Introduction

The production of synthetic natural gas (SNG) has been valued worldwide due to its promising prospect to solve energy problem. It has high conversion efficiency, and the existing gas distribution infrastructure can bring a lot of convenience. Coal can be converted into SNG by thermo-chemical processes. It contains gasification, gas cleaning and conditioning, followed by methanation of syngas, and subsequent gas upgrading.<sup>1</sup> Except for the methanation, other steps are not a problem due to the already industrialized processes such as ammonia synthesis, etc.

Therefore, Methanation has attracted great attention. It is a highly exothermic reaction:



From the thermodynamic respect, methanation favors low temperature and high pressure. However, operating at high pressure generates a large amount of heat. Thus the methanation technologies of existed SNG processes have a

series of reactors to remove the heat by adding intermediate or gas recycle cooling process.<sup>2</sup> G. Alex Mills et al.<sup>3</sup> concluded that CO methanation should be operated at the lowest temperatures that are consistent with acceptable catalyst activity, and with  $\text{H}_2/\text{CO}$  ratios at or above 3. Therefore, researches have long been focused on developing catalysts that are highly active at low temperature and stable at high temperature.

It is known that noble metals such as Pd, Rh, and Ru can catalyze methanation and exhibit high activity at low temperature.<sup>1,4</sup> Ni-based catalysts are commonly chosen for CO methanation due to their low cost, high catalytic activity and selectivity to methane. However, Ni-based catalysts are vulnerable to deactivate due to sintering and carbon deposition. CO dissociates quickly on Ni-based catalysts to form carbon intermediates, while the hydrogenation of the intermediates to generate  $\text{CH}_4$  is slow. Thus, carbon deposition leads to the deactivation of catalysts.<sup>4</sup> It was considered that Co catalysts tended to deposit carbon more than nickel catalysts under the

same operating conditions.<sup>3</sup> However, in the research of CO methanation mechanism over impregnated Co/Al<sub>2</sub>O<sub>3</sub> catalysts, the authors observed two steady-states for sulfur-free methanation over Co/Al<sub>2</sub>O<sub>3</sub> catalysts. And in the upper pseudo steady state, it showed very small amounts of carbon on the catalysts surface.<sup>5</sup>

Nanostructures exhibit excellent properties in electronic, optical, mechanical, and catalysis fields. Nanosized Co<sub>3</sub>O<sub>4</sub> is widely used in magnetism, photovoltaics, chemical sensors, and homogeneous catalysis. Large amounts of work has been done on the catalytic performance of nanosized Co<sub>3</sub>O<sub>4</sub> catalysts in low-temperature CO methanation,<sup>6</sup> Fischer-Tropsch (FT) synthesis,<sup>7,8</sup> low temperature CO oxidation,<sup>9,10</sup> selective reduction of nitrogen oxides,<sup>11</sup> and oxidation of arene derivatives.<sup>12,13</sup>

Co<sub>3</sub>O<sub>4</sub> is important oxide with spinel structure consisting of Co<sup>2+</sup> in a tetrahedral coordination and Co<sup>3+</sup> in an octahedral coordination, and O<sup>2-</sup> is cubic close packed. It has been demonstrated that metallic Co is the active phase for FT synthesis.<sup>8</sup> While for low temperature CO oxidation, Xie et al.<sup>9</sup> considered Co<sup>3+</sup> as the only active site. Zhu's group<sup>6</sup> believed Co<sup>3+</sup> and Co<sup>2+</sup> were the active sites for CO methanation together. Saputra et al.<sup>13</sup> thought Co<sup>3+</sup> and Co<sup>2+</sup> are active in generating hydroxyl radicals via Fenton-like reaction for advanced oxidation processes. In the selective catalytic reduction of nitrogen oxides with ammonia, Meng et al.<sup>11</sup> demonstrated that the high activity of Co<sub>3</sub>O<sub>4</sub> results from the Co<sup>3+</sup> species on the surface.

A lot of researchers focus on the preparation of different shapes of nano- Co<sub>3</sub>O<sub>4</sub>, including nanorods, nanoparticles, nanotubes, nanosheets, and nanowires.<sup>10,11,14,15</sup> It shows great discrepancy in catalytic activity among different shapes. Generally, Co<sub>3</sub>O<sub>4</sub> nanorods exhibit superior performance in CO oxidation and NO<sub>x</sub> reduction, which can be attributed to the abundant {110} planes that are rich in Co<sup>3+</sup> species. The conventional nanoparticles, which exposes mainly the {001} and {111} planes, contain only Co<sup>2+</sup> sites on the surface, appears to be less

active in NO<sub>x</sub> reduction and inactive in CO oxidation.<sup>9,11</sup> In formaldehyde oxidation, Co<sup>3+</sup> species on the {110} planes is also the active site.<sup>16</sup> Hu et al. reported that {112} planes perform excellent activity for methane oxidation.<sup>17</sup>

Literatures have reported that higher selectivity to CH<sub>4</sub> was observed in FT synthesis when Co catalysts were partially reduced or when the catalysts contained smaller Co<sub>3</sub>O<sub>4</sub> particles.<sup>6,7</sup> Zhu et al.<sup>6</sup> studied size effects of Co<sub>3</sub>O<sub>4</sub> nanoparticles for CO methanation in coke oven gas, As a result, it was found that smaller particle size of 20 nm performed excellently with the H<sub>2</sub>/CO ratio higher than 8.0. However, nanosized Co<sub>3</sub>O<sub>4</sub> for CO methanation in coal to SNG production, especially its preparation, structure and property in CO methanation, was not found in the open literature. Herein, we reported Co<sub>3</sub>O<sub>4</sub> nanoparticles with high catalytic activity for CO methanation in coal to SNG production, with H<sub>2</sub>/CO ratio of 3, low temperature of 300 °C, and high space velocity and pressure. It is demonstrated that CoO is the active phase for CO methanation through evaluating catalysts with different reduction degree.

## 2. Experimental

### 2.1 Preparation of Co<sub>3</sub>O<sub>4</sub>

Nanosized Co<sub>3</sub>O<sub>4</sub> was prepared via precipitation method. Cobalt nitrate hexahydrate (Kemiou chemical reagent Co. Ltd., Tianjin) was dissolved in ethylene glycol, and the mixture was gradually heated to 160 °C. Aqueous solution of 0.2 M (NH<sub>4</sub>)<sub>2</sub>CO<sub>3</sub> solution was then dropwise added. The slurry was stirred vigorously for 40 min with a continuous flow of nitrogen and aged for 0.5 h. After filtration and washing with deionized water, the solid was dried at 50 °C overnight under vacuum and calcined in air at 450 °C for 4 h. Catalyst for evaluation was consists of Co<sub>3</sub>O<sub>4</sub> and Al<sub>2</sub>O<sub>3</sub>, which were physically mixed. Typically, 1.3 g Co<sub>3</sub>O<sub>4</sub> powder was diluted with 1.3 g Al<sub>2</sub>O<sub>3</sub> powder. Thus approximately 2.6 g catalyst was used for each evaluation.

## 2.2 Catalyst characterization

### 2.2.1 N<sub>2</sub>-physisorption analysis

N<sub>2</sub> adsorption-desorption analysis of catalysts was conducted at liquid nitrogen temperature on a Tristar-3000 instrument (Micromeritics, United States). Prior to the analysis, catalysts were degassed first at 90 °C for 1 h and then at 300 °C for 3 h. The specific surface areas were determined by the multi-point Brunauer-Emmet-Teller (BET) method. The total pore volumes and sizes were evaluated using the standard Barrett Joyner Halenda (BJH) treatment.

### 2.2.2 Temperature programmed reduction analysis

The Temperature programmed reduction (TPR) analysis of the fresh catalyst was performed by the AutoChem 2910 analyzer (Micromeritics, United States). Prior to the TPR experiment, approximately 100 mg catalyst was pretreated with argon (99.99% pure) at 200 °C for 2 h to remove absorbed water and other contaminants. After the sample was cooled to 60 °C, a mixture of 10 vol.% H<sub>2</sub>/Ar was passed through the sample at a flow rate of 30 ml/min, and the temperature was increased to 1000 °C at a heating rate of 10 °C/min.

### 2.2.3 X-ray diffraction analysis

Powder X-ray diffraction (XRD) patterns were recorded on a D/max-2500 X-ray diffractometer (Rigaku, Japan) with a Ni-filtered Cu-K $\alpha$  radiation source ( $\lambda=1.54056$  Å) operated at 40 kV and 200 mA. The scanning angle was ranged from 10° to 90° with a speed of 8 °/min. The phase identification was determined by comparing with the Joint Committee on Powder Diffraction Standards (JCPDS).

### 2.2.4 X-ray photoelectron spectroscopy analysis.

X-ray photoelectron spectroscopy (XPS) analysis of all catalyst samples was performed using a PHI-1600 ESCA XPS system with monochromatic Mg-K $\alpha$  radiation and a chamber pressure of  $2 \times 10^{-10}$  Torr. The binding energies were calibrated to the C<sup>1s</sup> line at 284.6 eV. The peak areas were measured by a planimetric technique that assumed a linear baseline.

### 2.2.5 Transmission electron microscope analysis.

The Transmission electron microscope (TEM) images of the fresh and used catalysts were obtained with a Tecnai G<sup>2</sup>F20 (200 kV) transmission electron microscope (FEI, Holland). The samples were prepared via ultrasonic dispersion in ethanol at first. Then, a drop of the resultant suspension evaporated onto a holey copper grid.

### 2.2.6 TG analysis.

The coke analysis was performed via thermo-gravimetric (TG) experiments on a thermal analysis instrument (TG 209 F3 Tarsus). The experiments were carried out in a flow of air (30 mL/min) with a heating rate of 10 °C/min.

## 2.3 Catalyst reduction

To obtain different valence states of Co, different procedures of reduction were conducted prior to the methanation activity test. Catalyst (mixture of Co<sub>3</sub>O<sub>4</sub> and Al<sub>2</sub>O<sub>3</sub>) without reduction process was referred as cat.1. Correspondingly, catalysts reduced at 230 °C for 2 h and 450 °C for 4 h with H<sub>2</sub> flow rate of 100 mL/min were signed as cat.2 and cat.3, respectively.

## 2.4 Evaluation of catalytic activity

Catalytic activity tests were performed in a continuous flow fixed-bed reactor with a stainless steel tubular (12 mm I.D. and 700 mm in length). The catalyst was sieved and selected to 0.43-0.85 mm. The volume of each catalyst was 3.0 mL. The methanation reaction temperature and pressure were 300 °C and 3.0 MPa, respectively. A gas mixture containing 20% CO, 60% H<sub>2</sub>, and 20% N<sub>2</sub> was continuously passed through the catalysts at a space velocity of 11500 mL/g·h. The outlet gases were quantitatively analyzed by an online gas chromatograph (BEIFEN 3420A) equipped with a TCD and a FID. The conversion of CO, and selectivity to CH<sub>4</sub> was calculated using the following equations:

$$X_{\text{CO}} = \frac{F_{\text{CO,in}} - F_{\text{CO,out}}}{F_{\text{CO,in}}} \times 100\% \quad (1)$$

$$S_{\text{CH}_4} = \frac{F_{\text{CH}_4, \text{out}}}{F_{\text{CO}, \text{in}} - F_{\text{CO}, \text{out}}} \times 100\% \quad (2)$$

$$S_{\text{CO}_2} = \frac{F_{\text{CO}_2, \text{out}}}{F_{\text{CO}, \text{in}} - F_{\text{CO}, \text{out}}} \times 100\% \quad (3)$$

$$S_{\text{C}_2\text{H}_6} = \frac{2 \times F_{\text{C}_2\text{H}_6, \text{out}}}{F_{\text{CO}, \text{in}} - F_{\text{CO}, \text{out}}} \times 100\% \quad (4)$$

$$B_C = \frac{F_{\text{CO}, \text{in}} - F_{\text{CO}, \text{out}} - F_{\text{CH}_4, \text{out}} - F_{\text{CO}_2, \text{out}} - 2 \times F_{\text{C}_2\text{H}_6, \text{out}}}{F_{\text{CO}, \text{in}} - F_{\text{CO}, \text{out}}} \times 100\% \quad (5)$$

F refers to the flow rate (mL/min) of the gas in or out of the reactor,  $B_C$  refers to carbon balance.

### 3. Results

#### 3.1 Physicochemical properties of as-prepared nanosized $\text{Co}_3\text{O}_4$ sample

The BET specific surface area, pore volume and pore size of as-prepared  $\text{Co}_3\text{O}_4$  are listed in Table 1. The small BET surface area suggests that the as-prepared  $\text{Co}_3\text{O}_4$  is a non-perforated material. Fig. 1 shows the  $\text{N}_2$  isothermal adsorption-desorption profiles and pore distribution curves of nanosized  $\text{Co}_3\text{O}_4$ . The hysteresis loop indicates the profile is of type IV (IUPAC), revealing the mesoporous structure of the  $\text{Co}_3\text{O}_4$  sample. TEM image of the fresh as-prepared  $\text{Co}_3\text{O}_4$  is presented in Fig. 2 (a). The  $\text{Co}_3\text{O}_4$  particles are generally with rounded contours. It can be seen that the particle size of nano- $\text{Co}_3\text{O}_4$  is around 20-30 nm.

**Table 1.** Textural properties of nanosized  $\text{Co}_3\text{O}_4$

Catalyst	$S_{\text{BET}}$ ( $\text{m}^2/\text{g}$ )	$V_P$ ( $\text{cm}^3/\text{g}$ )	$D_P$ (nm)
$\text{Co}_3\text{O}_4$	41.4	0.17	13.80

$S_{\text{BET}}$ : BET specific surface area;  $V_P$ : pore volume;  $D_P$ : average pore diameter

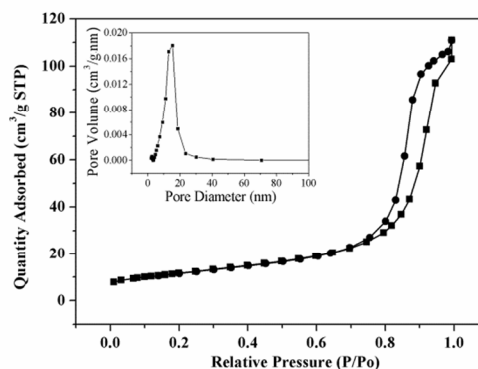


**Fig. 1**  $\text{N}_2$  adsorption-desorption profiles and pore distribution curves of nanosized  $\text{Co}_3\text{O}_4$

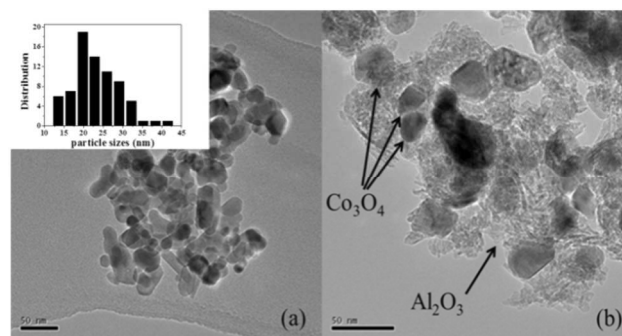


**Fig. 2** TEM images of (a) nanosized  $\text{Co}_3\text{O}_4$  and (b) catalyst of  $\text{Co}_3\text{O}_4$  diluted with  $\text{Al}_2\text{O}_3$  after 2h reduction at  $230^\circ\text{C}$

$\text{H}_2$ -TPR profiles of nanosized  $\text{Co}_3\text{O}_4$  is illustrated in Fig. 3. Two peaks are shown in the result. The lower temperature peak at around  $330^\circ\text{C}$  belongs to the reduction of  $\text{Co}^{3+}$  to  $\text{Co}^{2+}$ , and the higher temperature peak at  $480^\circ\text{C}$  is ascribed to the reduction of  $\text{Co}^{2+}$  to  $\text{Co}^0$ . The area of lower temperature peak is much smaller than the higher one, which demonstrates that  $\text{Co}^{3+}$  is reduced at first, and then the produced  $\text{Co}^{2+}$  and  $\text{Co}^{2+}$  in the catalyst itself are further reduced into metallic  $\text{Co}$ .<sup>16</sup> According to the TPR profile, reduction temperature of  $450^\circ\text{C}$  was used in the experiment to attain metallic  $\text{Co}$  before methanation reaction. To avoid excessive reduction,  $230^\circ\text{C}$  was adopted to obtain  $\text{CoO}$  from  $\text{Co}_3\text{O}_4$ .

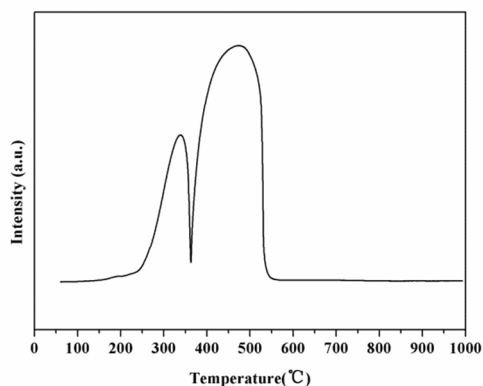


Fig. 3 H<sub>2</sub>-TPR profile of nanosized Co<sub>3</sub>O<sub>4</sub>

XRD pattern of nano-Co<sub>3</sub>O<sub>4</sub> is displayed in Fig. 4 (a). The results can be perfectly indexed into Co<sub>3</sub>O<sub>4</sub> of cubic phase with a lattice constant  $a=8.065\text{\AA}$ . No diffraction peaks related to impurities such as CoO are observed. Diffraction peaks at  $19^\circ$ ,  $31.3^\circ$ ,  $36.9^\circ$ ,  $38.6^\circ$ ,  $44.8^\circ$ ,  $55.6^\circ$ ,  $59.5^\circ$  and  $65.3^\circ$  ( $2\theta$ ) correspond to the {111}, {220}, {311}, {222}, {400}, {422}, {511} and {440} planes. Sharp peaks suggest the sample has a good crystallinity of pure Co<sub>3</sub>O<sub>4</sub> phase. The calculated crystallite size of Co<sub>3</sub>O<sub>4</sub> using the most intense peak at  $2\theta = 36.9^\circ$  ({311} plane) is 21 nm, which is consistent with the result of TEM analysis.

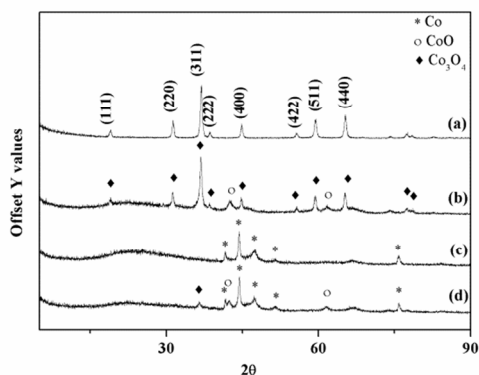


Fig. 4 XRD patterns of (a) nanosized Co<sub>3</sub>O<sub>4</sub>, (b) cat. 2 after reduction at 230 °C for 2 h, and (c) cat. 3 after reduction at 450 °C for 4 h, (d) cat. 1 before deactivation.

### 3.2 Characterization of catalysts after reduction

Catalysts (mixture of Co<sub>3</sub>O<sub>4</sub> and Al<sub>2</sub>O<sub>3</sub>) after reduction processes were also characterized with XRD. The results of XRD are shown in Fig. 4 (b) and (c), corresponding to cat.2 and cat.3, respectively. From Fig. 4 (b), it can be observed that after reduction at 230 °C for 2 h, diffraction peaks related to CoO at  $2\theta = 42.6^\circ$  and  $61.7^\circ$  appear. And intense peaks belong to Co<sub>3</sub>O<sub>4</sub> still exist. It indicates that Co<sub>3</sub>O<sub>4</sub> were partially reduced to CoO after the reduction process. While as presented in Fig. 4 (c), after reduction at 450 °C for 4 h, the characteristic peaks of metallic Co show up. No peaks of CoO or Co<sub>3</sub>O<sub>4</sub> can be detected, revealing the complete reduction of Co oxides. Thus it can be inferred that the components of cat.2 at the very beginning of methanation reaction are CoO and Co<sub>3</sub>O<sub>4</sub>. While for cat.3, metallic Co is the only existence form of Co species. No obvious peaks of Al<sub>2</sub>O<sub>3</sub> can be detected due to the superior crystallinity of metallic Co and Co oxides.

Fig. 2 (b) displays the TEM image of cat.2 after the reduction period of 2 h at 230 °C. It can be clearly observed that Co oxide particles uniformly mixed with Al<sub>2</sub>O<sub>3</sub>, and the reduction treatment didn't cause significant change to the Co oxide particles.

In addition, XPS analysis was used to evaluate the valence states of Co on the catalyst surface. Fig. 5 shows the deconvolution of Co 2p spectra for cat.1 and cat.2 before methanation reaction. The deconvolution of Co is difficult because of the existence of satellites peaks.<sup>19</sup> Co2p<sub>3/2</sub> has two components at B.E. = 779.6 and 781.4 eV, and Co2p<sub>1/2</sub> has two at B.E. = 794.9 and 796.7 eV, which related to Co<sup>3+</sup> and Co<sup>2+</sup> species, respectively.<sup>20</sup> It can be calculated that the ratio of Co<sup>3+</sup>/Co<sup>2+</sup> on the surface of cat.1 is 1.18. After being reduced at 230 °C for 2 h, the ratio of Co<sup>3+</sup>/Co<sup>2+</sup> decreases to 0.89 on the surface of cat.2. This indicates that part of surface Co<sup>3+</sup> species is reduced to Co<sup>2+</sup> after the mild reduction treatment, which is in accordance with XRD results.

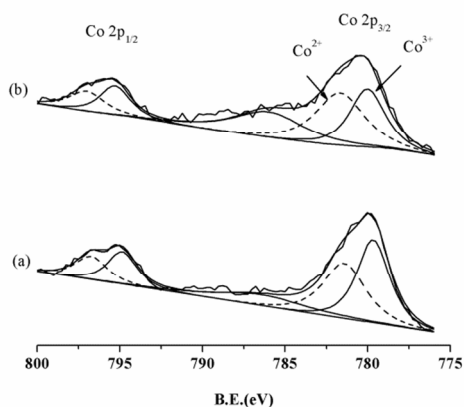


**Fig. 5** XPS patterns of (a) cat.1 without reduction and (b) cat. 2 after reduction at 230 °C for 2 h

### 3.3 Catalytic activity

The three catalysts with different reduction processes were evaluated for CO methanation reaction. The catalytic activities with time on stream are shown in Fig. 6. Cat.1 without reduction processing has an activation period of 3 h approximately. As the syngas used for methanation is of reducibility with 60 vol. % H<sub>2</sub>, it is deduced that a reduction reaction is proceeding during the activation period. Therefore, when the reduction reaction comes to a certain degree, catalyst becomes active for the CO methanation and soon achieves 100% conversion of CO, the selectivity to methane is 82%. Cat.2 suffered a mild reduction treatment shows excellent activity as soon as the syngas was input. It indicates that the mild reduction process prior to methanation can efficiently obtain the active phase for CO methanation. Cat.3 experienced a deep reduction process at 450 °C for 4 h. The evaluation results show that it is inactive for methanation reaction, revealing the absence of active phase. To certify the high activity of the catalyst originates from Co<sub>3</sub>O<sub>4</sub>, pure Al<sub>2</sub>O<sub>3</sub> was also tested and showed no catalytic activity at the same condition.

Another observation can be attained from Fig. 6. Cat.1 without reduction deactivated after evaluated for 7 h, while cat.2 keeps high activity with 100% conversion of CO throughout the evaluation period.

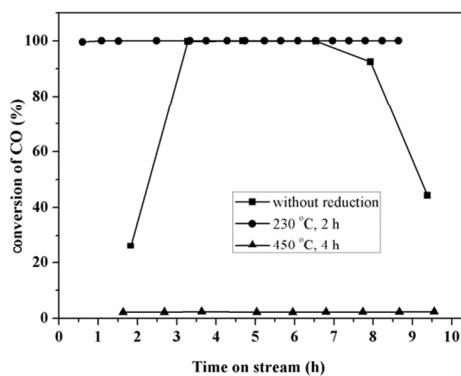
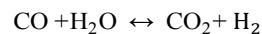


**Fig. 6** Catalytic performance with time on stream of catalysts after different reduction treatment

The selectivity of products was listed in table 2. As cat.3 had no methanation activity, the selectivity of cat.3 was not showed here. The displayed values were the average selectivity from 3 to 7 h on stream, during which time both catalysts performed excellent. It shows that cat.1 had a higher selectivity to methane than cat.2. It was because that at a reaction temperature of 300 °C, the actual temperature on the catalyst surface can be much higher than 300 °C. It would lead to the reduction of Co<sup>2+</sup> to metallic Co. While cat.2 undergone a pre-reduction treatment, the further reduction of Co species to metallic Co during methanation resulted in the lower selectivity to methane. On the other hand, more metallic Co contributes to the higher selectivity of long chain alkane, as the selectivity to C<sub>2</sub>H<sub>6</sub> revealed. It has to be explained that poor carbon balance of cat.2 is due to the generation of C<sub>3+</sub> hydrocarbons, which can also be attributed to the metallic Co.

However, Water Gas Shift (WGS) reaction also occurred on the catalysts surface, higher selectivity to CH<sub>4</sub> produced more H<sub>2</sub>O, thus promote the WGS reaction as follows:



Therefore, the selectivity to CO<sub>2</sub> was higher for cat.1 than cat.2 as depicted in table 2.

**Table 2.** Selectivity of catalysts

Catalyst	S <sub>CH4</sub>	S <sub>CO2</sub>	S <sub>C2H6</sub>	C balance
----------	------------------	------------------	-------------------	-----------

Cat.1	86.22	10.34	1.84	1.59
Cat.2	81.16	7.21	3.95	7.68

cat.1: without reduction; cat.2: reduced at 230 °C for 2 h.

### 3.4 Characterization of catalysts after evaluation

In order to study the deactivation of catalysts, TEM and TG-DTA were used to characterize the spent catalysts. Fig. 7 shows the results of the TG-DTA analysis of the spent catalysts after 10 h on stream. The TG curves can be divided into three regions: temperatures below 180 °C, 180–500 °C, and above 500 °C. The mass loss below 180 °C is due to the removal of moisture. The mass gain from 180 °C to 500 °C is attributed to the oxidation of the reduced Co species. It can be obtained from DTA results that this region includes two periods: temperature from 180 to 300 °C relate to the oxidation of metallic Co to CoO, temperature from 300 to 500 °C mainly refer to the oxidation of CoO to Co<sub>3</sub>O<sub>4</sub>. Divided peaks of cat.3 during 300 to 500 °C may due to the deep reduction of Co species at 450 °C, thus some metallic Co is difficult to be oxidized at lower temperature, and can be oxidized in this period. The slight mass loss above 500 °C is ascribed to the minimal carbon deposition during methanation evaluation. Compare the curves of three catalysts, cat.1 with a lower extent of reduction increases least in weight during the oxidation period in the second region. And cat.3 which experienced a deep reduction obtains a largest mass gain in the oxidation. The reduction extent of catalysts resulted in different amount of reduced Co species (Co<sup>2+</sup> and Co<sup>0</sup>), thus cause different degrees of mass increase in the oxidation period, which was fairly in accordance with the results of TG experiments. In the third region of above 500 °C, the slight loss of mass indicate that there is tiny carbon residual on the catalysts surface. However, the mass loss is less than 1% for all the spent catalysts, and the loss of cat.3 is relative larger. It is due to the absorbed CO was not transferred to hydrocarbons, and remained on the catalyst surface.

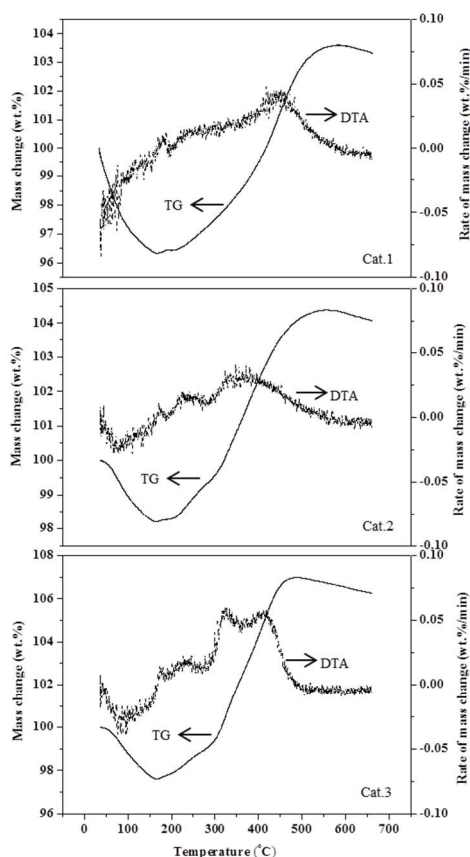


Fig. 7 TG-DTA profiles observed over used catalysts.

TEM images of cat.1 after evaluation are presented in Fig.8. Severe sintering of catalyst can be seen from Fig.8 (b). It is obvious that Co species aggregated after methanation reaction. However, a closer observation of catalyst surface in Fig.8 (a) revealed that no obvious carbon deposition occurred during methanation. The result is agreed with TG result. Therefore, sintering may be the main reason for catalyst deactivation.

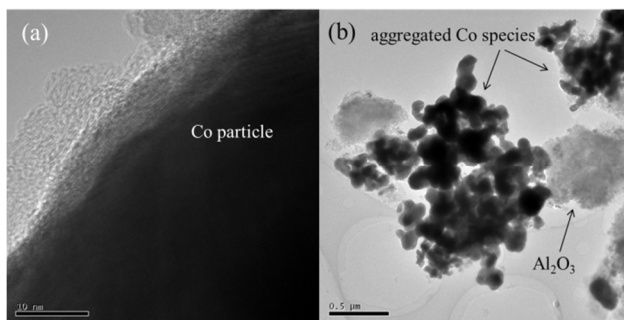


Fig. 8 TEM images of cat.1 after evaluation.

## 4. Discussion

### 4.1 Active phase of $\text{Co}_3\text{O}_4$ for methanation

It is generally accepted that the reduction of  $\text{Co}_3\text{O}_4$  to metallic Co undergoes two periods with a middle phase of CoO.<sup>7,20</sup>  $\text{Co}_3\text{O}_4$  is the active phase for CO oxidation, and metallic Co is the active phase for FT synthesis. Although CoO particles can easily exist under ambient room temperature and oxygen partial pressure, pure CoO is difficult to obtain by simple chemical route, it usually exist with small amount of  $\text{Co}_3\text{O}_4$  and Co metal.<sup>21</sup>

In our experiment, cat.1 without reduction maintained as  $\text{Co}_3\text{O}_4$  until the syngas was input. It didn't show any activity after feeding in syngas for 2 h. It can be deduced that  $\text{Co}_3\text{O}_4$  is not the active phase of CO methanation. However, after 3 h evaluation with a flow of syngas, cat.1 became highly active. It is believed that enough amount of active phase was generated after 3 h exposure of syngas, suggesting the active phase is the reduction state of  $\text{Co}_3\text{O}_4$ .

While for cat.3 with a complete reduction treatment, Co oxide turned to metallic Co before the methanation reaction, as the XRD results shown. As the atmosphere of methanation reaction is reductive, Co species of cat.3 should be metallic Co all long. Obviously, cat.3 didn't activate the methanation reaction in the whole evaluation period. Thus, it can be speculated that metallic Co is also not active for CO methanation.

Cat.2 experienced a mild reduction treatment, and CoO phase appeared after the reduction, as testified from the XRD and XPS results. It turned to be active immediately as the syngas was feed in. Therefore, it can be deduced that CoO is the active phase for CO methanation. To further prove the deduction, we obtained an evaluated cat.1 before deactivation, which experienced 4 h of evaluation. It was characterized with XRD as shown in Figure 4 (d). It can be observed that Co species on the active catalyst were  $\text{Co}_3\text{O}_4$ , CoO, and metallic Co. It clearly demonstrates that the catalyst reduction reaction from  $\text{Co}_3\text{O}_4$  to

Co happened during the methanation reaction process. Combining the evaluation with characterization results, it is found that catalyst performs active only in the presence of CoO phase. Without CoO, neither  $\text{Co}_3\text{O}_4$  nor metallic Co can catalyze the methanation reaction.

For CO oxidation, it is generally accepted that CO firstly adsorb on the surface  $\text{Co}^{3+}$ , and then  $\text{CO}_{\text{ads}}$  react with the oxygen species on  $\text{Co}_3\text{O}_4$ .<sup>9,22</sup> According to the literature<sup>9,11</sup>, the as-prepared  $\text{Co}_3\text{O}_4$  nanoparticles mainly expose {001} and {111} planes with vast  $\text{Co}^{2+}$  on the surface. However, from our experiments, since  $\text{Co}_3\text{O}_4$  is inactive at the initial stage, it can be deduced that  $\text{Co}^{2+}$  on the  $\text{Co}_3\text{O}_4$  nanoparticles is inactive for methanation. While  $\text{Co}^{2+}$  on the CoO surface is highly active for methanation reaction.

### 4.2 Mechanism of $\text{Co}_3\text{O}_4$ for methanation

Generally, there are two kinds of mechanisms proposed for CO methanation. The first is "carbide mechanism" by Fischer and Tropsch: CO first absorbed on the catalysts surface, and reduced to surface carbide  $\text{CH}_2^*$  by  $\text{H}_2$ . The second is "enolic complex" mechanism: absorbed CO and  $\text{H}_2$  form an enolic complex first,  $\text{H}_2$  then reduce the complex to form  $\text{CH}_2^*$ .<sup>3,5</sup> In spite of the discrepancy in intermediates, both of the two mechanisms consider CO and  $\text{H}_2$  adsorption as the first step, then a surface intermediate forms, and  $\text{H}_2$  react with the intermediate to generate  $\text{CH}_4$ .

Mills and Steffgen<sup>3</sup> mentioned that part of gas was irreversibly adsorbed on cobalt catalysts and this fraction did not participate in the formation of catalytic intermediates. We know from CO oxidation and other system that  $\text{Co}^{3+}$  can adsorb CO. However, we consider  $\text{Co}^{2+}$  on the CoO surface is active for the reaction of CO and  $\text{H}_2$  to generate  $\text{CH}_4$ . Thus it can be deduced that the adsorbed CO on  $\text{Co}^{3+}$  species was irreversible for the methanation reaction. And this will lead to less formation of active  $\text{Co}^{2+}$  sites for cat.1. However, a mild reduction process with  $\text{H}_2$  prior to methanation could ensure to generate enough amount of active  $\text{Co}^{2+}$ . When feeding in the syngas, the

abundant active  $\text{Co}^{2+}$  species immediately converted the adsorbed CO into methane. This cooperation can inhibit loss of active sites on catalyst surface, thus effectively improve the stability of catalyst.

## 5. Conclusions

In this report, the  $\text{Co}_3\text{O}_4$  nanoparticles showed high catalytic activity for low temperature CO methanation with  $\text{H}_2/\text{CO}$  ratio of 3, space velocity of 11500 mL/g·h and pressure of 3 MPa. By employing different reduction procedures, different Co species with various phases were obtained before methanation reaction. The above results and discussion indicates that the presence of CoO phase in  $\text{Co}_3\text{O}_4$  results in high activity for CO methanation. The mild reduction treatment can also improve the stability of catalyst.

## Acknowledgments

The authors gratefully acknowledge the financially support from the Ministry of Science and Technology of the People's Republic of China (Project 863- 2015AAJY1602).

## Notes and references

- 1 J. Kopyscinski, T. J. Schildhauer, S.M.A. Biollaz, *Fuel*, 2010, **89**, 1763-1783.
- 2 A. Zhao, W. Ying, H. Zhang, H. Ma, D. Fang, *Catal. Commun.*, 2012, **17**, 34-38.
- 3 G. A. Mills, F. W. Steffgen, *Catal. Rev. Sci. Technol.* 1974, **8**, 159-210.
- 4 X. Yan, Y. Liu, B. Zhao, Z. Wang, Y. Wang, C. J. Liu, *Int. J. Hydrogen Energ.*, 2013, **38**, 2283-2291.
- 5 P. K. Agrawai, J. R. Katzer, W. H. Manogue, *Ind. Eng. Chem. Fundam.* 1982, **21**, 385-390.
- 6 H. Zhu, R. Razaq, L. Jiang, C. Li, *Catal. Commun.*, 2012, **23**, 43-47.
- 7 C. Ahn, H. M. Koo, M. Jin, J. M. Kim, T. Kim, Y. W. Suh, K. J. Yoon, J. W. Bae, *Micropor. Mesopor. Mat.*, 2014, **188**, 196-202.
- 8 G. L. Bezemer, J. H. Bitter, H. P. C. E. Kuipers, H. Oosterbeek, J. E. Holewijn, X. D. Xu, F. Kapteijn, A. J. V. Dillen, K. P. D. Jong, *J. Am. Chem. Soc.*, 2006, **128**, 3956-3964.
- 9 X. Xie, Y. Li, Z. Q. Liu, M. Haruta, W. Shen, *Nature*, 2009, **458**, 746-749.
- 10 C. Liu, Q. Liu, L. Bai, A. Dong, G. Liu, S. Wen, *J. Mol. Catal. A: Chem.*, 2013, **370**, 1-6.
- 11 B. Meng, Z. Zhao, X. Wang, J. Liang, J. Qiu, *Appl. Catal. B: Environ.*, 2013, **129**, 491-500.
- 12 D. Qiao, C. Xu, J. Xu, *Catal. Commun.*, 2014, **45**, 44-48.
- 13 E. Saputra, S. Muhammad, H. Sun, H. M. Ang, M. O. Tade, S. Wang, *J. Colloid Interf. Sci.*, 2013, **407**, 467-473.
- 14 Y. Lv, Y. Li, W. Shen, *Catal. Commun.*, 2013, **42**, 116-120.
- 15 K. S. Hui, K. N. Hui, C. L. Yin, X. Hong, *Mater. Lett.*, 2013, **97**, 154-157.
- 16 Q. Yan, X. Li, Q. Zhao, G. Chen, *J. Hazard. Mater.*, 2012, **209-210**, 385-391.
- 17 C. Ma, D. Wang, W. Xue, B. Dou, H. Wang, Z. Hao, *Environ. Sci. Technol.*, 2011, **45**, 3628-3634.
- 18 C. Li, Y. Shen, M. Jia, S. Sheng, M. O. Adebajo, H. Zhu, *Catal. Commun.*, 2008, **9**, 355-361.
- 19 D. Laurenti, B. Phung-Ngoc, C. Roukoss, E. Devers, K. Marchand, L. Massin, L. Lemaitre, C. Legens, A-A. Quoineaud, M. Vrinat, *J. Catal.*, 2013, **297**, 165-175.
- 20 B. Bai, H. Arandiyani, J. Li, *Appl. Catal. B: Environ.*, 2013, **142-143**, 677-683.
- 21 Q. S. Guo, X.Y. Guo, Q. H. Tian, *Adv. Powder Technol.*, 2010, **21**, 529-533.
- 22 H.F. Wang, R. Kavanagh, Y. L. Guo, Y. Guo, G. Z. Lu, P. Hu, *Angew. Chem. Int. Edit.*, 2012, **51**, 6657-6661.